Research Article

Fatemah H. Alkallas, Amira Ben Gouider Trabelsi, Kholoud Saad Almugren, Asmaa M. Elsayed*, and Mohamed Rabia*

Porous sponge-like AsOI/poly(2-aminobenzene-1-thiol) nanocomposite photocathode for hydrogen production from artificial and natural seawater

https://doi.org/10.1515/ntrev-2025-0221
received December 31, 2024; accepted September 11, 2025

Abstract: The direct conversion of seawater into hydrogen fuel represents a promising advancement in the pursuit of sustainable and renewable energy sources. In this study, we report the fabrication and characterization of a novel arsenic oxoiodide/poly(2-aminobenzene-1-thiol) (AsOI/P2ABT) nanocomposite photocathode with a distinctive sponge-like morphology. The composite exhibits hierarchical porosity with pore sizes ranging from ~50 to 700 nm, along with a granulated surface uniformly decorated with ~20 nm nanoparticles with a promising bandgap of 2.76 eV. The AsOI/P2ABT photocathode demonstrates significant potential for industrial-scale hydrogen generation by employing both natural and artificial seawater in a three-electrode photoelectrochemical cell. The system achieved hydrogen evolution rates of approximately 4.2 and 4.0 μmol/h cm² for artificial and natural seawater, respectively. Under full-spectrum white light illumination, the current densities in light (J_{ph}) reached −0.103 and −0.105 mA/cm², indicating comparable performance between the two electrolytes. These findings highlight the practicality of using natural seawater as a low-cost, abundant, and environmentally benign electrolyte. The study underscores the viability of the AsOI/P2ABT photocathode for direct seawater-to-hydrogen conversion, offering a scalable and eco-friendly approach to renewable hydrogen fuel production.

Keywords: arsenic oxoiodide, poly(2-aminobenzene-1-thiol), renewable energy, hydrogen, nanocomposite

1 Introduction

The growing global demand for sustainable and efficient energy solutions has intensified research into renewable energy sources. Replacing traditional fossil fuels is becoming increasingly urgent due to their severe environmental impacts, including the emission of SO_X, CO_X, and NO_X gases, which contribute to global warming, air pollution, and ecological degradation [1,2]. A transition to clean energy is essential to mitigate these harmful effects and support long-term environmental sustainability [3].

Among the various renewable options, solar energy stands out as one of the most promising due to its abundance, versatility, and adaptability across different applications. In recent decades, solar-driven photocatalysis has emerged as a powerful method for generating hydrogen gas (H_2) – a clean, high-energy fuel with wide-ranging applications in industrial processes, residential energy systems, and transportation [4,5]. Photocatalytic hydrogen generation involves splitting water molecules into hydrogen and oxygen using solar irradiation, and significant progress has been made in enhancing the efficiency of this process by developing novel photocatalytic materials [6].

One of the most effective strategies for improving photocatalyst performance is to engineer nanostructured materials, such as core–shell architectures, nanowires, and porous frameworks. These designs increase the surface area, promote charge separation, and enhance light absorption and reaction kinetics [7,8]. However, despite extensive research, only a limited number of materials meet the essential requirements for efficient hydrogen evolution – namely, strong light absorption, thermal stability, and appropriate bandgap energy for electron excitation and mobility [9,10].

To overcome these limitations, researchers have explored conductive and conjugated polymers as

* **Corresponding author: Asmaa M. Elsayed**, TH-PPM Group, Physics Department, Faculty of Science, Beni-Suef University, Beni-Suef, 62514, Egypt, e-mail: asmaa.elsayed@science.bsu.edu.eg
* **Corresponding author: Mohamed Rabia**, Nanomaterials Science Research Laboratory, Chemistry Department, Faculty of Science, Beni-Suef University, Beni-Suef, 62514, Egypt,
e-mail: mohamedchem@science.bsu.edu.eg
Fatemah H. Alkallas, Amira Ben Gouider Trabelsi, Kholoud Saad Almugren: Department of Physics, College of Science, Princess Nourah Bint Abdulrahman University, P.O. Box 84428, Riyadh, 11671, Saudi Arabia

alternative materials for photocatalysis. These polymers offer several advantages, including simple synthesis routes, cost-effectiveness, and high electrochemical conductivity [11]. Among them, conjugated polymers are especially promising due to their extended π-electron systems, which allow for broader light absorption and improved charge transport. Earlier studies have shown that composites like polyaniline (PANI)/PbS and PANI/graphene oxide exhibit photocatalytic activity, although their hydrogen generation efficiency remains modest [12,13]. This has driven further innovation in hybrid systems that combine polymers with metal oxides or other inorganic materials.

A particularly promising direction involves the development of polymer–metal oxide nanocomposites, which exhibit synergistic properties ideal for photocatalytic applications. These hybrids often possess optimized bandgap energies (~1.2 eV) suitable for solar-driven water splitting. However, the photocatalytic performance of such systems is heavily influenced by the choice of electrolyte, as it affects both the photocurrent density and electrode stability. Common electrolytes like $NaBH_4$, NH_4OH, H_2SO_4, and KOH are effective but can accelerate corrosion and limit the operational lifespan of the photocathode [14–16]. Furthermore, their reliance on freshwater raises sustainability concerns.

To address these challenges, there is growing interest in identifying alternative electrolytes that are not only effective but also environmentally benign and aligned with the principles of green chemistry. Seawater, both natural and artificial, has emerged as a promising candidate due to its abundance and suitability for large-scale applications, provided the electrode materials are stable and efficient under such conditions [17,18].

The present study introduces a novel AsOI/P2ABT nanocomposite as a high-performance photocathode for hydrogen generation from natural and artificial seawater. The composite is synthesized through a two-step process involving the oxidative polymerization of 2-aminobenzene-1-thiol (P2ABT), followed by its reaction with sodium meta-arsenite ($NaAsO_2$) to incorporate arsenic oxide (AsOI). The resulting sponge-like nanostructure provides a high surface area and facilitates efficient light absorption and charge transfer.

AsOI contributes to the composite by modifying the optical and electronic properties of the polymer matrix. Its incorporation leads to enhanced light-harvesting capabilities and improved electron–hole separation due to favorable band alignment. P2ABT, a conjugated polymer, offers excellent conductivity, chemical stability, and functional groups that interact effectively with metal oxides, making it an ideal host for AsOI integration. Together, these materials form a synergistic system capable of driving efficient hydrogen evolution.

Comprehensive characterization techniques, including SEM, TEM, cross-sectional imaging, and spectroscopic analysis, confirm the successful formation of the nanocomposite and elucidate its morphology, crystallinity, and chemical bonding. Photoelectrochemical performance was evaluated in a three-electrode system, using both natural and artificial seawater as electrolytes. The composite demonstrated comparable hydrogen generation and photocurrent densities in both cases, highlighting its potential for scalable and sustainable green hydrogen production. This study not only validates the performance of the AsOI/P2ABT nanocomposite but also emphasizes the feasibility of using natural seawater as an eco-friendly and cost-effective electrolyte for future energy applications.

2 Materials and methods

2.1 Materials

Sodium arsenite ($NaAsO_2$, 99.9%, Pio-Chem), 2-aminobenzene-1-thiol (99.9%, Merck, Germany), iodine (I_2, 99.9%, Pio-Chem), potassium iodide (KI, 99.9%, Pio-Chem), hydrochloric acid (36%, Merck, Germany), ammonium persulfate ($(NH_4)_2S_2O_8$, 99.9%; Pio-Chem), and acetic acid (CH_3COOH, 99.9%, El-Nasr, Egypt) were used.

2.2 Preparation of the AsOI/P2ABT nanocomposite

To prepare the AsOI/P2ABT nanocomposite, the 2-aminobenzene-1-thiol monomer undergoes direct oxidation using iodine dissolved in potassium iodide as the oxidant. This reaction is performed with a molar ratio of 1:2.5, where the monomer concentration is set at 0.06 M. Acetic acid serves as the acidic medium for dispersing the monomer. The reaction occurs at room temperature and continues for over 24 h, during which polymerization is completed. Simultaneously, AsOI is incorporated into the P2ABT polymer matrix. The coordination bonds between AsOI and the polymer signify the successful synthesis of this thin film nanocomposite, which deposits on a glass slide.

Additionally, the pristine P2ABT polymer synthesis follows similar steps, with the 2-aminobenzene-1-thiol monomer directly oxidized using $(NH_4)_2S_2O_8$ in an HCl medium.

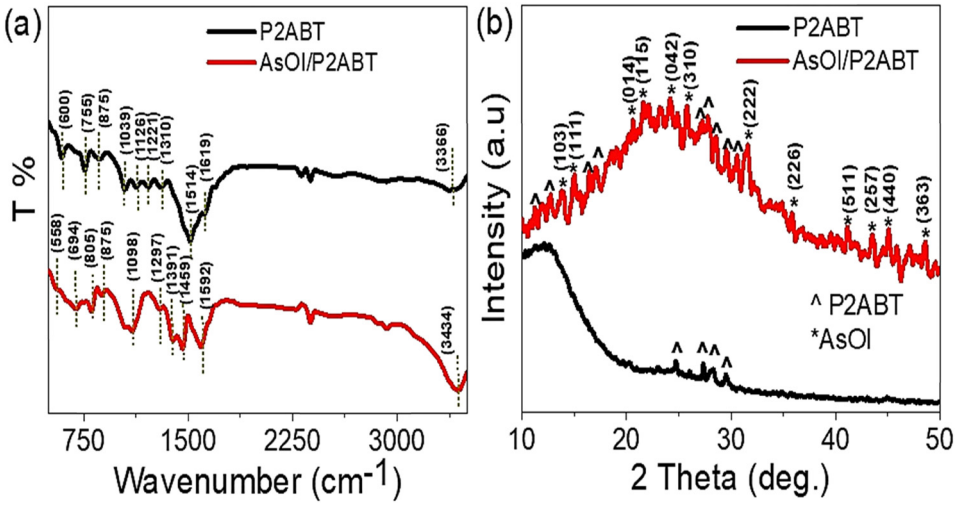

Figure 1: The chemical structure of the AsOI/P2ABT nanocomposite based on (a) FTIR spectra and (b) XRD patterns.

2.3 Green hydrogen generation with the AsOI/P2ABT nanocomposite photocathode

The AsOI/P2ABT nanocomposite photocathode is tested for H_2 production from Red Sea water as an electrolyte. It is considered a sustainable, available, and low-cost electrolyte source, containing natural ions like sodium (Na), magnesium (Mg), and calcium (Ca), which act as self-sacrificing agents in the process. A synthetic seawater solution with a similar composition is prepared to investigate these ions' influence. This enables a detailed evaluation of how the specific ions and anions affect hydrogen generation. The solution contains NaCl (38.3 g/l), $CaCl_2$ (2.4 g/l), $MgCl_2$ (19.0 g/l), Na_2SO_4 (5.2 g/l), and $KHCO_3$ (0.2 g/l) [19].

In the assembled cell, the AsOI/P2ABT photocathode is utilized as the working electrode, where the reduction process occurs, and the current density (J_{ph}) is measured as an indicator of hydrogen gas generation at this photocathode. This reduction releases electrons, which are quantified using a CHI608E workstation. Faraday's law is then applied, as shown in equation (1) [20]. The hydrogen generated is calculated by measuring the baseline dark current (J_o).

A metal halide vacuum tube with a 400 W white light source illuminates the system to facilitate this measurement. The light intensity is modulated using optical filters, producing photon energies of 3.6, 2.8, 2.3, and 1.7 eV. These variations in light intensity allow for precise control over the illumination conditions. This experimental setup effectively evaluates the photocathode sensitivity to photons, which is critical for efficient and rapid H_2 gas. The three-electrode setup is estimated in Figure S1.

$$H_2\text{mole} = \int_0^t J_{ph} \cdot dt/F. \quad (1)$$

3 Results and discussion

3.1 Physicochemical characterization

The FTIR data of the synthesized AsOI/P2ABT nanocomposite provide strong evidence of AsOI incorporation into the P2ABT network, supporting the formation of this composite, as shown in Figure 1(a). This integration plays a key role in the vibrational bending behavior observed, affecting both bending vibrations and spatial configuration within the composite. The shifts in FTIR band intensity and position effectively indicate this incorporation.

The ring structure of P2ABT displays various functional groups identified by FTIR spectroscopy at specific wavenumbers: 1,039, 1,126, 1,221, 1,310, 1,514, and 1,619 cm^{-1}. These peaks shift in the composite, appearing at 1,098, 1,297, 1,391, 1,459, and 1,592 cm^{-1}, which confirms structural interaction. Additional external groups, such as N–H and S–H, appear at 3,366 cm^{-1} in pristine P2ABT and shift to 3,434 cm^{-1} in the AsOI/P2ABT composite.

Similarly, the out-of-plane C–H bending is seen at 875 and 755 cm^{-1} in the pristine polymer and shifts to 875 and 805 cm^{-1} in the composite. The observed variations in the peak positions and intensities confirm the successful integration of AsOI into the P2ABT structure, supporting the formation of the nanocomposite. Specifically, the shift of the P2ABT band from 600 to 694 cm^{-1} in the composite, along with the appearance of a new broad band at 558 cm^{-1}, indicates strong interactions between AsOI and the functional groups of P2ABT (Table 1).

The crystalline properties of the synthesized AsOI/P2ABT nanocomposite were characterized using XRD analysis, revealing distinct peaks at various positions, as shown in Figure 1(b). These peaks highlight the crystallinity of the composite, which is enhanced by incorporating AsOI into the P2ABT matrix. Twelve peaks appear at 13.8°, 15.0°, 20.6°, 21.5°, 24.2°, 25.8°, 31.6°, 36.0°, 41.1°, 43.6°, 45.0°, and 48.7°, corresponding to the crystallographic planes (103), (111), (104), (115), (042), (310), (222), (226), (511), (257), (440), and (363), as indexed in the JCPDS card 23-1519 [23], and confirm the successful integration of AsOI within the P2ABT structure, forming a stable crystalline AsOI/P2ABT composite.

Additionally, nine peaks between 11.3° and 30.6° are characteristic of the P2ABT component, reflecting its crystalline structure and contribution to the composite. In contrast, the pristine P2ABT alone shows peaks only between 24.6° and 30.5°, indicating a more limited crystalline range compared to the composite. This increase in crystalline peaks and broad range in the AsOI/P2ABT composite demonstrates an improvement in crystallinity due to AsOI incorporation, with coordination bonds forming throughout the polymer chains.

The AsOI material also improves the composite's optical properties, improving its performance for photon capture within its internal layers. This heightened crystallinity and light-trapping ability make the AsOI/P2ABT composite suitable for photocatalytic applications, especially in green hydrogen production. Thus, the enhanced crystalline structure supports the composite's potential applications in various sustainable energy solutions, where efficient light absorption and photocatalytic activity are key for maximizing performance.

The AsOI/P2ABT nanocomposite structure is thoroughly examined through XPS analysis to determine the oxidation states of the inorganic components integrated within the composite, as shown in Figure 2. This analysis also enabled the identification of key elements in the pristine P2ABT polymer. In the survey spectrum in Figure 2(a), distinct peaks are observed for nitrogen (N) at 400 eV, associated with specific N transitions in the organic P2ABT, and for carbon (C) at 285.8 eV, confirming the C-related transitions. Also, sulfur (S) is identified with a peak at 162.8 eV, as shown in Figure 2(d). These signals validate the presence of organic elements in P2ABT, forming part of the composite structure.

Table 1: FTIR band positions of the AsOI/P2ABT composite and pristine P2ABT polymer

Function group	Group position (cm^{-1})	
	AsOI/P2ABT	**P2ABT**
N–H and S–H [21]	3,434	3,366
P2ABT ring [22]	1,592, 1,459, 1,391, 1,297, and 1098	1,619, 1,514, 1,310, 1,221, 1,126, and 1,039
C–H out	875 and 805	875 and 755
As–O–I	558	—

The inorganic component of the composite, which includes arsenic (As) and iodine (I) in combination with oxygen (O), is also clearly verified through XPS. Oxygen, for example, is identified by its characteristic peak at 532 eV, as shown in Figure 2(a). Arsenic is present in two distinct transitions, $As3d_{5/2}$ and $As3d_{7/2}$, which appear at binding energies of 42.9 and 44.5 eV, respectively, providing evidence of the As oxidation state and bonding environment. Figure 2(c) further confirms the presence of iodine, with $I3d_{5/2}$ and $I3d_{3/2}$ transitions visible at 618.4 and 629.9 eV, respectively [24]. Together, these As and I signals indicate the formation of the AsOI compound, which is embedded within the P2ABT matrix.

The presence of these elements – N, C, S from the P2ABT and As, I, O from the AsOI – along with their corresponding oxidation states, supports the conclusion that AsOI is successfully integrated into the P2ABT network. This integration likely occurs through coordination bonds, resulting in a stable AsOI/P2ABT nanocomposite structure. The detailed XPS analysis provides chemical bonds and confirms the successful formation of the composite, with each element contributing to the composite's overall stability and potential functional applications.

The photocatalytic efficiency of the AsOI/P2ABT nanocomposite is rooted in its exceptional ability to absorb a substantial amount of incident photons. This characteristic is evident from the absorbance curve depicted in Figure 3(a), which highlights notable differences in photon absorption behavior between pristine P2ABT and the AsOI/P2ABT nanocomposite.

In pristine P2ABT, the absorption spectrum exhibits a narrower, sharper peak in the UV-Vis region, extending up to 430 nm, accompanied by an additional peak in the visible (Vis) region reaching 640 nm. Conversely, due to a small, broad peak in the Vis region, the AsOI/P2ABT nanocomposite demonstrates a significantly broader absorption range, from 280 nm to approximately 500 nm and further to 680 nm. These peaks arise from electron transitions through the π–π* interaction [25]. The enhanced absorption capacity of the nanocomposite, covering over 50% of the solar spectrum, is highly promising for advancing its role in various optical and photocatalytic applications. This curve indicates that the composite exhibits significant absorption primarily in the UV–Vis region, while its

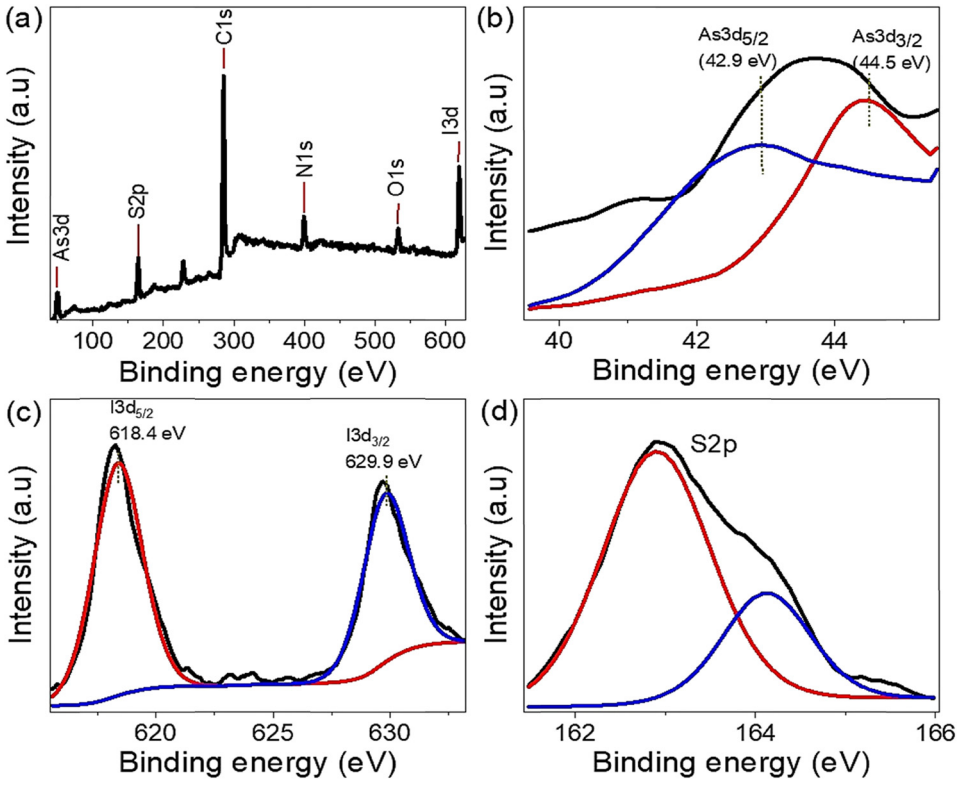

Figure 2: XPS analysis of the synthesized AsOI/P2ABT nanocomposite showing (a) the overall survey scan, (b) arsenic, (c) iodine, and (d) sulfur elements.

absorbance in the infrared (IR) range is minimal. This suggests that the material interacts with IR radiation mainly through bond vibrational modes, rather than electronic transitions. To further evaluate the optical properties of these materials, the Tauc equation (2) [26,27] is used. This approach utilizes the absorbance coefficient and the general absorbance (A) across the UV–Vis and Vis regions to estimate the optical bandgap (E_g). The analysis revealed E_g values of 3.15 eV for the pristine P2ABT polymer and 2.76 eV for the AsOI/P2ABT nanocomposite. The reduced bandgap in the composite indicates improved optical performance attributed to the integration of AsOI within the P2ABT polymer matrix. This enhancement underscores the potential of the AsOI/P2ABT nanocomposite as an efficient material for photocatalytic and other optoelectronic applications, benefiting from its superior light absorption and tailored electronic properties.

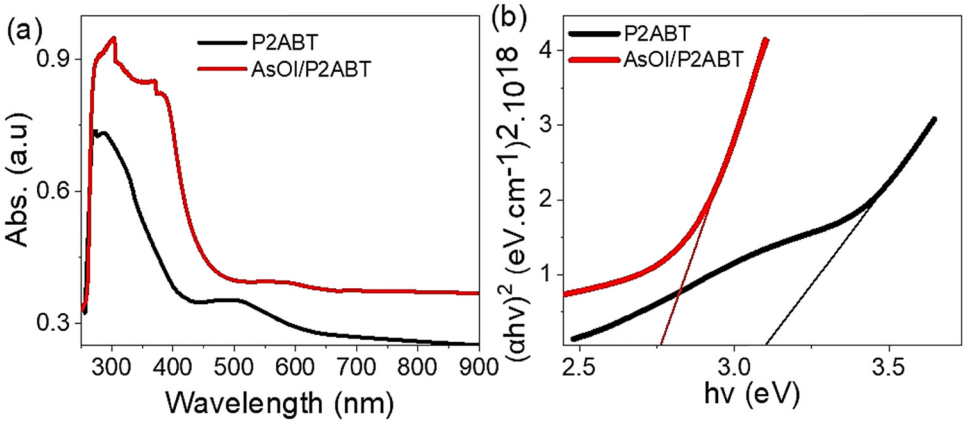

Figure 3: Comparative optical properties of the synthesized AsOI/P2ABT nanocomposite and the pristine P2ABT polymer: (a) the absorption spectrum and (b) the corresponding bandgap values.

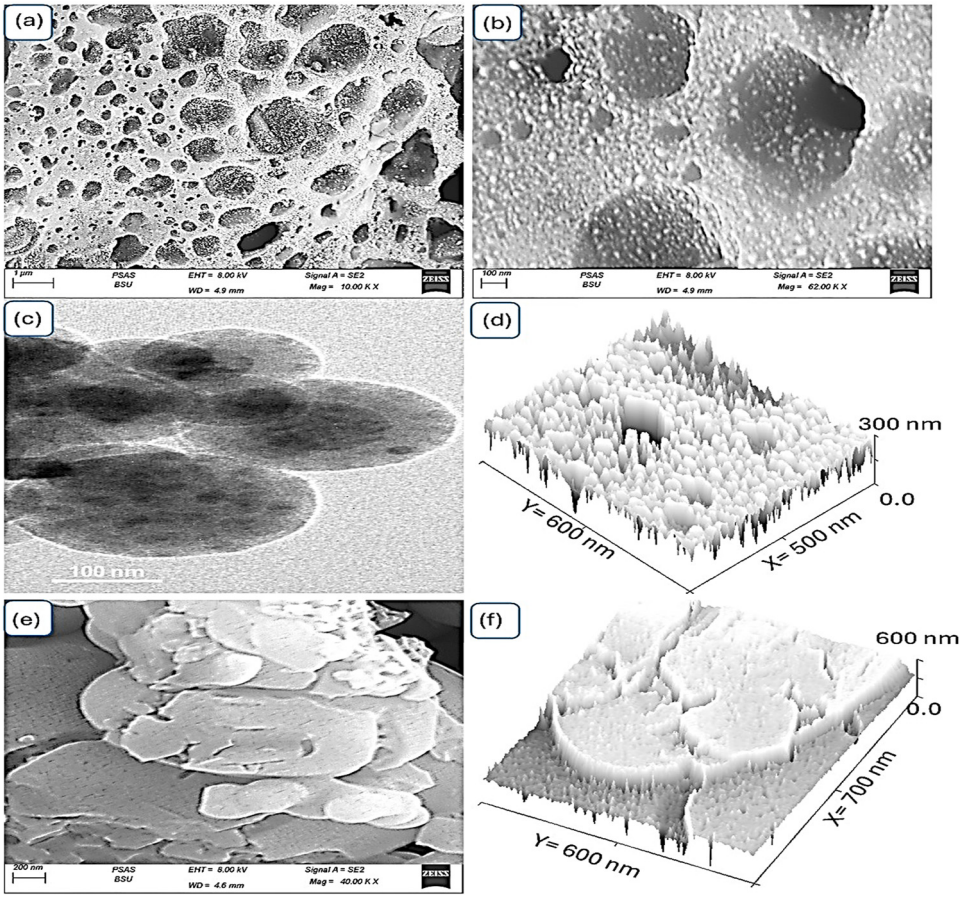

Figure 4: Morphological analysis of the AsOI/P2ABT nanocomposite using (a) and (b) SEM at different magnifications, (c) TEM for material blending, and (d) cross-sectional roughness. Additionally, (e) SEM and (f) cross-section of the pristine P2ABT polymer are presented for comparison.

$$\alpha h\nu = A(h\nu - E_g)^{\frac{1}{2}}. \quad (2)$$

The AsOI/P2ABT nanocomposite exhibits a close relationship between its morphological and optical properties, making it essential to analyze its structure for a deeper understanding of its functionality. The morphological characteristics are examined using SEM for a detailed 3D perspective, as shown in Figure 4(a) and (b) under varying magnifications. The AsOI/P2ABT nanocomposite exhibits a sponge-like morphology characterized by pores with a diameter of about ~ 50–700 nm, separated by a granulated surface coated with nanoparticles of ~20 nm. This rough and porous structure significantly enhances the active surface area, making it highly beneficial for photocatalysis and hydrogen gas (H_2) generation. The surface roughness is attributed to small granules distributed on the sponge-like framework and pores within the structure.

Further insights were gained from TEM imaging, which confirmed the homogeneous integration of materials in the nanocomposite. The dark regions observed in the TEM images correspond to the AsOI material embedded within the P2ABT matrix, indicating a seamless blend of components (Figure 4(c)). The cross-sectional morphology of the nanocomposite was also analyzed, with theoretical calculations based on the SEM images estimating an average granule size of 20 nm. Additionally, nanoscale pores were observed to be uniformly dispersed between the particles, further enhancing their functional properties (Figure 4(d)).

In comparison, the SEM analysis of the pristine P2ABT polymer (Figure 4(e)) revealed a distinct morphology comprising large, clefted spherical particles. Theoretical modeling (Figure 4(f)) confirmed this formation, highlighting the absence of nanoscale particles or the porous structure seen in the composite. This is performed using the simulation program, Gwyddion, which processes real SEM images to provide enhanced clarity, including a 3D cross-sectional view. The pristine P2ABT lacks the enhanced surface features in the nanocomposite, which are critical for its improved photocatalytic performance. These findings underscore the transformative impact of AsOI integration on the morphology and functionality of the P2ABT

polymer. The particle distribution of the AsOI/P2ABT nanocomposite and the P2ABT particles is shown in Figure S2(a) and (b), respectively. This analysis reveals that the composite exhibits a narrower distribution range compared to the P2ABT alone.

3.2 Green hydrogen (H_2) generation from natural or artificial seawater using the AsOI/P2ABT photocathode

The AsOI/P2ABT photocathode demonstrates significant potential for green hydrogen (H_2) generation under full-spectrum white light and distinct monochromatic lights. This innovative process involves an electrochemical cell, where the AsOI/P2ABT photocathode facilitates the reduction reaction necessary for H_2 production. The system uses natural Red Sea water (electrolyte), a highly sustainable and cost-effective resource. Utilizing seawater reduces dependence on freshwater and opens avenues for industrial-scale hydrogen generation through economical and eco-friendly methods.

In addition to its economic advantages, natural seawater offers a technical edge by providing ionic species that enhance charge mobility. These ions contribute to the OH radicals' provision, producing hydrogen gas. To ensure the ions in seawater function solely as sacrificial agents without contributing to undesired side reactions, the system was tested with artificial seawater. This artificial medium replicates the chemical composition of natural seawater but excludes heavy metals. Testing under these conditions confirms that the photocathode operates efficiently for water splitting without interference from heavy metal reduction processes.

The AsOI/P2ABT photocathode's performance is rooted in its chemical and physical properties. The photocathode is a composite of inorganic arsenic AsOI and the P2ABT polymer, interconnected chemically to form a robust network. This structure supports a synergistic coordination mechanism that enhances the material's semiconductor behavior. The composite facilitates efficient charge transfer, with photogenerated charge carriers (electron–hole pairs) separating effectively: electrons accumulate on the surface of AsOI, while holes concentrate on P2ABT. This separation creates a potential gradient and an electric field that spans the semiconductor, driving the water-splitting reaction [28–30].

Additionally, the polymer matrix of P2ABT provides remarkable chemical corrosion resistance. This property ensures the longevity of the photocathode and protects the external surface when AsOI is embedded within the polymer. This durability is crucial for practical applications, particularly under prolonged exposure to challenging electrolytic environments like seawater.

The photocathode's performance was evaluated under two electrolytes: natural Red Sea water and equivalent artificial seawater. These tests were conducted under both white light and dark conditions. The results, illustrated in Figure 5, show minimal differences in the photocathode's performance between the two electrolytes. The dark current density (J_o) values were −0.029 and −0.032 mA/cm^2 for natural and artificial seawater, respectively, while J_{ph} values were −0.103 and −0.105 mA/cm^2. These results indicate that the absence of heavy metals in artificial seawater does not significantly affect the water-splitting process, and seawater ions primarily facilitate hydrogen generation. The J_{ph} value of this promising AsOI/P2ABT composite with an unusual electrolyte is greater than those reported in the literature for TiN–TiO_2 or CuO–C/TiO_2 [31]. The AsOI/P2ABT photocathode demonstrates excellent potential for sustainable hydrogen production. Its efficient charge transfer, corrosion resistance, and compatibility with natural seawater make it a promising pave the way toward eco-friendly and cost-effective green energy solutions.

The estimated bandgap value of 2.76 eV is a critical factor for assessing the light-responsive behavior of the AsOI/P2ABT nanocomposite. This parameter influences the material's performance under varying light sources, as indicated by the corresponding variation in the produced current (Figure 6). The variation in responsivity stems from the differing energies of photons interacting with the composite material, leading to energy splitting. The AsOI/P2ABT nanocomposite exhibits distinct responses

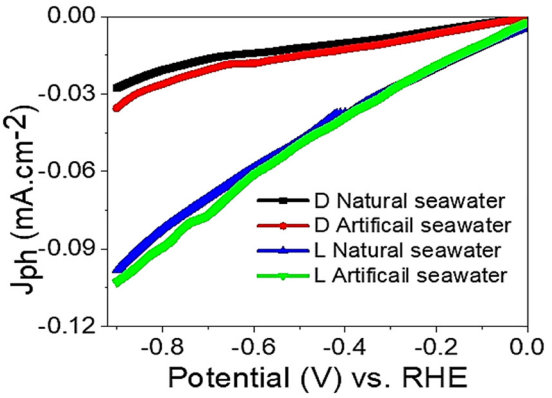

Figure 5: The electrochemical performance of the AsOI/P2ABT photocathode evaluated under different electrolyte solutions, comparing natural seawater and artificial seawater.

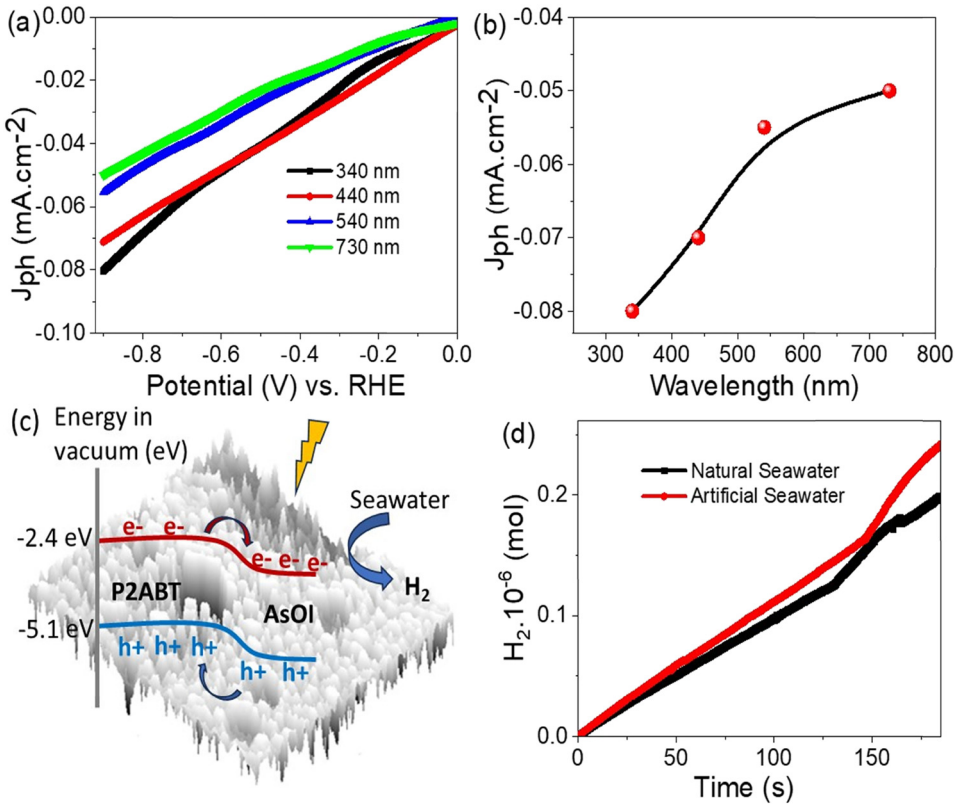

Figure 6: The performance of the fabricated AsOI/P2ABT photocathode under various monochromatic light sources: (a) potential *versus* current-density relationship and (b) the corresponding current density values at −0.9 V displayed in a bar chart. (c) The mechanism of electron and hole transfer within the system, and (d) the amount of H_2 gas produced by the AsOI/P2ABT photocathode during seawater splitting.

to these photons, as reflected in the evaluated photocurrent density values.

Photon wavelengths of 440 and 340 nm, with energy values exceeding the bandgap, demonstrate a marked difference in behavior compared to 730 and 540 nm, which possess lower energy levels. This distinction is evident in Figure 6(a), where the J_{ph} values under 340 and 440 nm illumination are estimated to be −0.08 and −0.072 mA/cm², respectively. Conversely, under 540 and 730 nm illumination, the J_{ph} decreased to −0.053 and −0.05 mA/cm². These results are summarized in Figure 6(b), offering a clear visualization of the variations in the photocurrent density across different wavelengths.

This behavior highlights the fabricated AsOI/P2ABT photocathode's optimal performance for splitting Red Sea seawater in UV and the initial Vis light regions. These two spectral regions possess sufficient photon energies to excite the composite material, initiating significant electron generation. The excited photons create a "cloud" of hot electrons that populate the external energy levels of the composite, forming a robust electric field around the material [32,33]. This electric field efficiently transfers electrons to the adjacent seawater, driving the water splitting and enabling the generation of hydrogen gas.

This process involves the interaction of photons within the UV and visible light ranges with the AsOI/P2ABT nanocomposite, which absorbs the incoming energy. This absorption excites electrons, pushing them to higher energy states, thereby creating a significant electric potential. The robust electric field generated by this process effectively directs the flow of hot electrons toward the seawater interface. At this interface, the electrons participate in water's electrochemical splitting and hydrogen gas liberation.

This process is estimated by the movement of charge carriers in the AsOI/P2ABT photocathode that follows a distinct pattern. P2ABT has a lowest unoccupied molecular orbital (LUMO) at −2.4 eV [34]. These energy levels make P2ABT a suitable hole transport material (HTM) and an electron donor upon illumination. On the other hand, arsenic oxoiodide (AsOI), a hybrid oxide/iodide material, functions primarily as the photoabsorber and electron transport material. While the CB position of AsOI is around −5.1 eV, the total bandgap of this composite is 2.76 eV, as

shown in Figure 3(b). Holes predominantly migrate toward the P2ABT material, accumulating on its surface, while electrons are transferred in the opposite direction. This dynamic charge separation and transport process is visually depicted in Figure 6(c). Such behavior is crucial for the photocathode's functionality, ensuring effective charge utilization during the water-splitting reaction.

Furthermore, the photocathode's hydrogen gas production rate was calculated to be approximately 4.2 and 4.0 μmol/h cm^2 using the artificial and natural seawater, as shown in Figure 6(d). This estimation is derived using Faraday's law (equation (1)), which correlates the charge transfer with the amount of H_2 generated. This production rate is notably promising compared to recent studies involving similar materials. For instance, photocathodes based on composites like polypyrrole/NiO_X [35], polypyrrole/graphene oxide [36], and poly(m-toluidine)/roll-GO [37] typically achieve H_2 generation rates of around 2.0 μmol/h cm^2.

The observed differences in the photocurrent density between wavelengths indicate the composite's selective light absorption and its ability to harness energy efficiently within specific spectral ranges. The higher J_{ph} values under UV and short-wavelength visible light suggest that the AsOI/P2ABT photocathode is well-suited for applications requiring high energy input, such as hydrogen generation through seawater splitting. This characteristic underscores the composite's potential for renewable energy applications, offering an effective means of utilizing solar energy for sustainable hydrogen production with a promising behavior as evaluated in Table 2. In addition, to further evaluate H_2 gas generation over an extended period (3,650 s), the performance of the AsOI/P2ABT photocathode in producing hydrogen gas from both natural and artificial seawater over a longer duration was assessed (Figure S3).

The photocathodic behavior of pristine P2ABT is illustrated in Figure S4, where its performance was assessed in natural seawater. The measured J_{ph} was relatively low, approximately −0.03 mA cm^{-2}. This modest value reflects the limited photoresponse of P2ABT when used alone, without any enhancement in the AsOI component. The absence of AsOI, which plays a crucial role in charge separation and light absorption, significantly reduces the overall efficiency of the photocathode. These findings emphasize the importance of incorporating AsOI to improve the photocatalytic activity and validate the synergistic effect observed in the composite structure.

The EIS analysis of the AsOI/P2ABT photocathode in natural seawater is illustrated in the Nyquist plot (Figure S5). The plot exhibits a semicircular region followed by a steep increase at higher impedance values. The semicircle corresponds to the charge transfer process at the photocathode–electrolyte interface, and its diameter reflects the charge transfer resistance (R_{CT}) of 80 Ω. The moderate size of this semicircle indicates that the AsOI/P2ABT composite enables relatively efficient charge transfer, which is essential for photocatalytic hydrogen evolution. The sharp increase at higher Z' values suggests the presence of Warburg impedance, typically associated with ion diffusion limitations in the electrolyte. Overall, the EIS profile confirms the effective photoelectrochemical behavior of the AsOI/P2ABT electrode in seawater, supporting its potential use in green hydrogen production applications.

Table 2: Performance of the AsOI/P2ABT photocathode in seawater splitting compared to other studies

Photoelectrode	Electrolyte	J_{ph} (mA/cm^2)
Poly(m-aminobenzoic acid) [38]	H_2SO_4	0.08
CuO/TiO_2 [31]	Glycerol	0.012
Polypyrrole/NiO [35]	Sewage water	0.09
Cr_2O_3–$Cr(OH)_3$/poly-2-chloroaniline [39]	Seawater	0.02
ZnO [40]	Na_2SO4	0.05
Polypyrrole/graphene oxide [36]	Sewage water	0.08
SnO_2–ZnO/g-C_3N_4 [41]	Glycerol	—
AsOI/P2ABT photocathode (this work)	Artificial seawater	0.105
AsOI/P2ABT photocathode (this work)	Natural seawater	0.103

4 Conclusions

This study demonstrates the fabrication of an AsOI/P2ABT nanocomposite photocathode with a sponge-like morphology. The composite exhibits a bandgap of 2.76 eV, enabling effective light absorption in the UV and initial visible regions. The material features pores ranging from approximately 50 to 700 nm, with a granulated surface covered by nanoparticles of around 20 nm in diameter. The crystallite structure, metal oxidation, and groups of the synthesized material are thoroughly analyzed using various characterization techniques.

Hydrogen generation was successfully achieved using both natural and artificial seawater in a three-electrode cell system, producing approximately 4.2 μmol/h cm^2 of H_2 gas from artificial seawater and 4.0 μmol/h cm^2 from natural seawater. Under full white light illumination, the evaluated J_{ph} values were −0.103 mA/cm^2 for artificial

seawater and −0.105 mA/cm² for natural seawater, indicating comparable performance between the two electrolytes. Additionally, the photocathode's sensitivity is evaluated under various light wavelengths, showing higher current densities at 340 and 440 nm, decreasing performance at longer wavelengths (540 and 730 nm). The significant advantages of utilizing natural seawater, such as cost-effectiveness, abundance, and eco-friendly properties, are important to this study. These attributes make natural seawater a highly suitable and practical electrolyte for direct H_2 gas production using the AsOI/P2ABT photocathode, providing a promising pathway for large-scale renewable energy applications.

Acknowledgments: The authors express their gratitude to Princess Nourah bint Abdulrahman University Researchers Supporting Project number (PNURSP2025R223), Princess Nourah bint Abdulrahman University, Riyadh, Saudi Arabia.

Funding information: This research was funded by Princess Nourah bint Abdulrahman University Researchers Supporting Project number (PNURSP2025R223), Princess Nourah bint Abdulrahman University, Riyadh, Saudi Arabia.

Author contributions: All authors have accepted responsibility for the entire content of this manuscript and approved its submission.

Conflict of interest: The authors state no conflict of interest.

Data availability statement: All data generated or analyzed during this study are included in this published article.

References

[1] Tsao CW, Narra S, Kao JC, Lin YC, Chen CY, Chin YC, et al. Dual-plasmonic Au@Cu7S4 yolk@shell nanocrystals for photocatalytic hydrogen production across visible to near infrared spectral region. Nat Commun. 2024;15:1–13. doi: 10.1038/s41467-023-44664-3.

[2] de Kleijne K, Huijbregts MAJ, Knobloch F, van Zelm R, Hilbers JP, de Coninck H, et al. Worldwide greenhouse gas emissions of green hydrogen production and transport. Nat Energy. 2024;2024:1–14. doi: 10.1038/s41560-024-01563-1.

[3] Oshiro K, Fujimori S. Limited impact of hydrogen co-firing on prolonging fossil-based power generation under low emissions scenarios. Nat Commun. 2024;15:1–11. doi: 10.1038/s41467-024-46101-5.

[4] Alnuwaiser MA, Rabia M, Elsayed AM. Paving the way for commercial hydrogen generation from natural and artificial seawater based on photocathode of manganese(II) oxide–manganese(IV) oxide/poly–1H pyrrole nanocomposite seeded on additional poly–1H pyrrole film. Int J Energy Res. 2025;2025:9369233. doi: 10.1155/ER/9369233.

[5] Abdulaziz F, Zayed M, Latif S, Jeilani YA, Shaban M, Patel RRD, et al. Fabrication of gold/polyaniline/copper oxide electrode for efficient photoelectrochemical hydrogen evolution. Phys Chem Chem Phys. 2025;7:100094. doi: 10.1039/D5CP00350D.

[6] Ben A, Trabelsi G, Rabia M, Alkallas FH, Kusmartsev FV. Polypyrrole-bismuth tungstate/polypyrrole core-shell for optoelectronic devices exhibiting Schottky photodiode behavior. Sci Rep. 2024;14:27651.

[7] ur Rehman MN, Munawar T, Nadeem MS, Mukhtar F, Maqbool A, Riaz M, et al. Facile synthesis and characterization of conducting polymer-metal oxide based core-shell PANI-Pr2O–NiO–Co3O4 nanocomposite: As electrode material for supercapacitor. Ceram Int. 2021;47:18497–509. doi: CERAMINT.2021.03.173">10.1016/J.CERAMINT.2021.03.173.

[8] Elsayed AM, Alkallas FH, Trabelsi ABG, Rabia M. Highly uniform spherical MoO2-MoO3/polypyrrole core-shell nanocomposite as an optoelectronic photodetector in UV, Vis, and IR Domains. Micromachines. 2023;14:1694. doi: 10.3390/MI14091694.

[9] Chauhan P, Siraj S, Joseph KS, Dabhi S, Bhadu GR, Sahatiya P, et al. Synergistically driven CoCr-LDH@VNiS2 as a bifunctional electrocatalyst for overall water splitting and flexible supercapacitors. ACS Appl Mater Interfaces. 2023;15:32515–24. doi: 10.1021/ACSAMI.3C03115/SUPPL_FILE/AM3C03115_SI_001.PDF.

[10] Pataniya PM, Sumesh CK. MoS_2 nanosheets on Cu-foil for rapid electrocatalytic hydrogen evolution reaction. J Electroanalytical Chem. 2022;912:116270. doi: JELECHEM.2022.116270">10.1016/J.JELECHEM.2022.116270.

[11] Tuan DD, Huang CW, Duan X, Lin CH, Lin KYA. Cobalt-based coordination polymer-derived hexagonal porous cobalt oxide nanoplate as an enhanced catalyst for hydrogen generation from hydrolysis of borohydride. Int J Hydrogen Energy. 2020;45:31952–62. doi: IJHYDENE.2020.08.243">10.1016/J.IJHYDENE.2020.08.243.

[12] Rabia M, Mohamed HSH, Shaban M, Taha S. Preparation of polyaniline/PbS core-shell nano/microcomposite and its application for photocatalytic H2 electrogeneration from H_2O. Sci Rep. 2018;8:1107. doi: 10.1038/s41598-018-19326-w.

[13] Shaban M, Rabia M, El-Sayed AMA, Ahmed A, Sayed S. Photocatalytic properties of PbS/graphene oxide/polyaniline electrode for hydrogen generation. Sci Rep. 2017;7:1–13. doi: 10.1038/s41598-017-14582-8.

[14] Baydaroglu FO, Özdemir E, Gürek AG. Polypyrrole supported Co–W–B nanoparticles as an efficient catalyst for improved hydrogen generation from hydrolysis of sodium borohydride. Int J Hydrogen Energy. 2022;47:9643–52. doi: IJHYDENE.2022.01.052">10.1016/J.IJHYDENE.2022.01.052.

[15] Li Z, Huang G, Wang Y, Lu C, Huang H, Kou J. Pyroelectric effects in CdS phase junctions for dual-enhanced photocatalytic hydrogen production. Catal Sci Technol. 2023;13:2559–65. doi: 10.1039/D3CY00210A.

[16] Sun B, Li X, Zheng J. Hydrogen generation from NaBH4 for portable proton exchange membrane fuel cell. Mater Rep: Energy. 2024;4:100248. doi: 10.1016/J.MATRE.2023.100248.

[17] Alqahtani MS, Mohamed SH, Hadia NMA, Rabia M, Awad MA. Some characteristics of Cu/Cu2O/CuO nanostructure heterojunctions and

their applications in hydrogen generation from seawater: effect of surface roughening. Phys Scr. 2024;99:045939. doi: 10.1088/1402-4896/AD30B3.
[18] Pelayo D, Pérez-Peña E, Rivero MJ, Ortiz I. Shedding light on the photocatalytic hydrogen generation from seawater using CdS. Catal Today. 2024;433:114672. doi: 10.1016/J.CATTOD.2024.114672.
[19] Moradi-Alavian S, Kazempour A, Mirzaei-Saatlo M, Ashassi-Sorkhabi H, Mehrdad A, Asghari E, et al. Promotion of hydrogen evolution from seawater via poly(aniline-co-4-nitroaniline) combined with 3D nickel nanoparticles. Sci Rep. 2023;13:1–10. doi: 10.1038/s41598-023-48355-3.
[20] Alkallas FH, Mahmoud A, Abd M, Ben A, Trabelsi G. Eminent Red Sea water hydrogen generation via a Pb (II) -iodide/poly (1H -pyrrole) nanocomposite photocathode. Green Process. Synth. 2024;13(1):20240048. doi: 10.1515/gps-2024-0048.
[21] Azzam EMS, Abd El-Salam HM, Aboad RS. Kinetic preparation and antibacterial activity of nanocrystalline poly(2-aminothiophenol). Polym Bull. 2019;76:1929–47. doi: 10.1007/S00289-018-2405-Z/FIGURES/14.
[22] Atta A, Abdeltwab E, Negm H, Al-Harbi N, Rabia M, Abdelhamied MM. Characterization and linear/non-linear optical properties of polypyrrole/NiO for optoelectronic devices. Inorg Chem Commun. 2023;152:110726. doi: 10.1016/J.INOCHE.2023.110726.
[23] Zhong GQ, Zhong WW, Jia RR, Jia YQ. Solid-state synthesis, characterization, and biological activity of the bioinorganic complex of aspartic acid and arsenic triiodide. J Chem. 2013;2013:217947. doi: 10.1155/2013/217947.
[24] Rabia M, Aldosari E, Moussa M. Bird nest-like shape of polypyrrole-iodide/iodine complex nanocomposite with highly optical and morphological behavior for green hydrogen generation. Indian J Phys. 2024;2024:1–10. doi: 10.1007/S12648-024-03353-7.
[25] Tian J, Xue Q, Yao Q, Li N, Brabec CJ, Yip HL. Inorganic halide perovskite solar cells: progress and challenges. Adv Energy Mater. 2020;10:2000183. doi: 10.1002/aenm.202000183.
[26] Haryński Ł, Olejnik A, Grochowska K, Siuzdak K. A facile method for Tauc exponent and corresponding electronic transitions determination in semiconductors directly from UV–Vis spectroscopy data. Opt Mater. 2022;127:112205. doi: 10.1016/J.OPTMAT.2022.112205.
[27] Baishya K, Ray JS, Dutta P, Das PP, Das SK. Graphene-mediated band gap engineering of WO3 nanoparticle and a relook at Tauc equation for band gap evaluation. Appl Phys A: Mater Sci Process. 2018;124:1–6. doi: 10.1007/S00339-018-2097-0/FIGURES/5.
[28] Almutairi MM, Ebraheim EE, Mahmoud MS, Atrees MS, Ali MEM, Khawassek YM. Nanocomposite of TiO_2@ Ni- or Co-doped graphene oxide for efficient photocatalytic water splitting. Egypt J Chem. 2019;62:1649–58. doi: 10.21608/EJCHEM.2019.9722.1648.
[29] Rana MM, Alam KM, Chaulagain N, Garcia J, Kumar N, Vrushabendrakumar D, et al. Tunable absorption and emission in mixed halide bismuth oxyhalides for photoelectrochemical water splitting. ACS Appl Nano Mater. 2024;7:6005–19. doi: 10.1021/ACSANM.3C05925/SUPPL_FILE/AN3C05925_SI_001.PDF.
[30] Zhao Q, Liu Z, Guo Z, Ruan M, Yan W. The collaborative mechanism of surface S-vacancies and piezoelectric polarization for boosting CdS photoelectrochemical performance. Chem Eng J. 2022;433:133226. doi: 10.1016/J.CEJ.2021.133226.
[31] Huang X, Zhang M, Sun R, Long G, Liu Y, Zhao W. Enhanced hydrogen evolution from CuOx-C/TiO2 with multiple electron transport pathways. PLoS One. 2019;41(4):0215339. doi: 10.1371/JOURNAL.PONE.0215339.
[32] Podder S, Pal AR. Plasmonic visible-NIR photodetector based on hot electrons extracted from nanostructured titanium nitride. J Appl Phys. 2019;126:083108. doi: 10.1063/1.5101009.
[33] Naldoni A, Guler U, Wang Z, Marelli M, Malara F, Meng X, et al. Broadband hot-electron collection for solar water splitting with plasmonic titanium nitride. Adv Opt Mater. 2017;5:1601031. doi: 10.1002/adom.201601031.
[34] Tsai HW, Hsueh KL, Chen MH, Hong CW. Electronic and Optical Properties of Polythiophene Molecules and Derivatives. Crystals. 2021;11:1292. doi: 10.3390/CRYST11111292.
[35] Atta A, Negm H, Abdeltwab E, Rabia M, Abdelhamied MM. Facile fabrication of polypyrrole/NiOx core-shell nanocomposites for hydrogen production from wastewater. Polym Adv Technol. 2023;34(5):1633–41. doi: 10.1002/PAT.5997.
[36] Hamid MMA, Alruqi M, Elsayed AM, Atta MM, Hanafi HA, Rabia M. Testing the photo-electrocatalytic hydrogen production of polypyrrole quantum dot by combining with graphene oxide sheets on glass slide. J Mater Sci: Mater Electron. 2023;34:1–11. doi: 10.1007/S10854-023-10229-9/METRICS.
[37] Helmy A, Rabia M, Shaban M, Ashraf AM, Ahmed S, Ahmed AM. Graphite/rolled graphene oxide/carbon nanotube photoelectrode for water splitting of exhaust car solution. Int J Energy Res. 2020;44:7687–97. doi: 10.1002/er.5501.
[38] Modibane KD, Waleng NJ, Ramohlola KE, Maponya TC, Monama GR, Makgopa K, et al. Poly(3-aminobenzoic acid) decorated with cobalt zeolitic benzimidazolate framework for electrochemical production of clean hydrogen. Polymers. 2020;12:1581. doi: 10.3390/polym12071581.
[39] Trabelsi ABG, Elsayed AM, Alkallas FH, Rabia M. Flower-like Cr_2O_3-$Cr(OH)_3$/poly-2-chloroaniline nanocomposite photoelectrode grown on polypyrrole film for hydrogen generation from sewage water. Opt Quantum Electron. 2024;56:1–14. doi: 10.1007/S11082-023-05306-6/METRICS.
[40] Al-saeedi SI. Photoelectrochemical green hydrogen production utilizing ZnO nanostructured photoelectrodes. Micromachines. 2023;14(5):1047. doi: 10.3390/mi14051047.
[41] Vattikuti SVP, Anil P, Reddy K, Shim J, Byon C. Visible-light-driven photocatalytic activity of SnO_2 − ZnO quantum dots anchored on g - C_3N_4 nanosheets for photocatalytic pollutant degradation and H_2 production. ACS Omega. 2018;3(7):7587–602. doi: 10.1021/acsomega.8b00471.